ELSEVIER

Polymer 40 (1999) 1657–1666

polymer

Morphology, phase continuity and mechanical behaviour of polyamide 6/chitosan blends

Alain Dufresne[a,*], Jean-Yves Cavaillé[a], Danièle Dupeyre[a], Marcela Garcia-Ramirez[b], Jorge Romero[c]

[a]*Centre de Recherches sur les Macromolécules Végétales (CERMAV), CNRS, Université Joseph Fourier, BP 53, 38041 Grenoble cedex 9, Cedex, France*
[b]*Industrias NEGROMEX S.A. de C.V. P.O. Box 257-c, 89000 Tampico, Tam., Mexico*
[c]*Centro de Investigacion en Quimica Aplicada (CIQA), P.O. Box 379-c, 25100 Saltillo, Coah, Mexico*

Received 18 April 1997; revised 2 March 1998; accepted 29 April 1998

Abstract

Blends of chitosan with polyamide 6 (PA6) were prepared via the solution casting technique using formic acid as a common solvent. The morphology and the mechanical behaviour of films with chitosan concentrations ranging from 15% to 70% (*w*/*w*) were investigated by scanning electron microscopy and dynamic mechanical analysis. Assuming an hypothesis about blend morphology, the mechanical behaviour of the materials was predicted from various models involving the percolation concept. From comparison between experimental and predicted data it is concluded that the chitosan phase tends to sediment and to form a continuous phase on the lower face of the film, if the chitosan content is high enough. This continuous phase is bristling with chitosan domain cones, which can emerge on the upper face of the film depending on the blend composition. The PA6 rich domains fill the upper face of the sample. © 1999 Elsevier Science Ltd. All rights reserved.

Keywords: Morphology; Phase continuity; Mechanical behaviour

1. Introduction

Chitin is one of the most abundant polysaccharides found in nature. It is a biodegradable, renewable biomass macromolecule that has the same β-(1 → 4)-D-glucopyranose units backbone as cellulose. However, in contrast with cellulose, the 2-hydroxy is replaced by an acetamide group, resulting in mainly β-(1 → 4)-2-acetamido-2-deoxy-)-D-glucopyranose structural units (GLcNAc)[1]. Chitosan is the *N*-deacetylated derivative of chitin, though this *N*-deacetylation is almost never complete. Different batches of chitosan vary according to the degree of polymerization and degree of deacetylation. Commercially available materials are generally deacetylated to about 80%, with an ill-defined distribution of acetylamide residues[2]. Therefore, chitosan is an heteropolymer.

Many reviews have been written which outline chitin and its derivatives' usefulness in such areas as pharmaceutical and biomedical applications, paper production, textile finishes, photographic products, cements, heavy metal chelating agents, membranes, hollow fibres, and in waste removal[1,3–5].

Investigation of blends and composites of conventional thermoplastic polymers with naturally occurring macromolecules, or their derivatives, is a broad area of material science that is very rich in potential. In particular, modification of chitosan by means of blending with other polymers is a convenient and effective method of improving physical properties for practical utilization. In particular, it has been reported that the hydrophilic properties of chitosan can be modified by blending with poly(vinyl alcohol) [6]. Films of chitosan–nylon-4 blends show good mechanical properties and retain the excellent chelating ability of chitosan[7]. It has been observed that the compatibility and morphology of chitosan–poly(ethylene oxide) blends are closely related to the composition. Below 50% (*w*/*w*) chitosan the two parent polymers are miscible, and above this composition the blends are phase-separated[8]. Blends of chitosan with strongly crystalline polyamides (nylon-4 and nylon-6) and weakly crystalline polyamides (caprolactam/lauroactam and Zytel®) were also investigated[9]. Their characterization suggests partial miscibility of chitosan with nylon-4 and lack of miscibility in other polyamides. Moreover, blending with nylon-4 enhances mechanical properties with marked antiplasticization in blends contain-

* Corresponding author.

0032-3861/99/$ - see front matter © 1999 Elsevier Science Ltd. All rights reserved.
PII: S0032-3861(98)00335-8

ing 90% chitosan, and catalytic activity of the chitosan is enhanced.

Polymer blends are most often found to be multiphase systems[10], due mainly to the very small value of the mixing entropy. The consequence of such a feature is that a negative free energy of mixing requires a negative enthalpy of mixing and this is known to occur for only few examples[11]. However, an understanding of the macroscopic properties of multiphase systems cannot be deduced solely from the properties of each phase, as is often the case for homogeneous blends. They also depend on the spatial organization of each phase, and on the characteristics of interfaces.

Among the various macroscopic properties, dynamic mechanical data can be used to study the morphology, i.e. the phase continuity and the miscibility of a polymer blend. It is a powerful tool:

1. to determine the glass–rubber transition temperature for the different amorphous phases and so their average composition;
2. to give information on the type of domain morphology (matrix-inclusions, connectivity of the more rigid phase…) and their respective volume fraction; and
3. in some cases, to detect the presence of interphase between the main phases of the blends[10,12].

The plot of the storage modulus at a given temperature versus composition can be related to models which allow predictions of phase continuity and phase inversion in a polymer blend.

In the present study, blends of chitosan and polyamide 6 (PA6) have been prepared by casting films from a common solvent. Morphology and mechanical properties are investigated for various blend compositions, using scanning electron microscopy (SEM), dynamic mechanical analysis and modelling of the mechanical response of the material.

2. Experimental

2.1. Materials

Polyamide 6 (PA6) was provided as pellets by Celanese Mexicana. Its average molecular weights determined by g.p.c. were $\overline{M}_n = 46\,800$ and $\overline{M}_w = 80\,600$[13]. The chitosan used was a commercial material obtained from crab shell (Polyscience, Inc.). Its degree of deacetylation was experimentally determined by *FT*i.r. and was 71%. The common solvent used was formic acid purchased from Aldrich (USA).

2.2. Polyamide 6/chitosan blends processing

Polymers were first dried under vacuum for 15 h at 80°C and kept in a desiccator over P_2O_5. Polyamide 6 and chitosan were then dissolved together in formic acid (1% *w*/*w*) at room temperature with stirring for 4 h. Translucid films were obtained by casting and evaporating these solutions to produce blends with final compositions 100/0, 85/15, 50/50, 30/70 and 0/100 (*w*/*w*), the first number referring to PA6 throughout this work. The evaporation step was performed at 60°C during 4 h. Resulting films, which thickness ranged from 10 to 50 μm, were finally freeze-dried.

2.3. Scanning electron microscopy

Scanning electron microscopy (SEM) was performed to investigate the morphology of the materials with a JEOL JSM-6100 instrument. The upper and lower surfaces of the films were coated with gold on a JEOL JFC-1100E ion sputter coater and observed. The SEM was operated using secondary electrons at 7 kV.

Three sets of samples were observed. The first corresponds to as evaporated and coated films and the two other to films submitted to an etching treatment prior to coating. The films were treated either with *m*-cresol in order to remove PA6 from the surface or to chitinases which are known to remove chitin and its derivatives. In fact, these etching treatments consist of three-step processes:

1. films were immersed in *m*-cresol for 48 h at room temperature with magnetic stirring. Because *m*-cresol is a good solvent for PA6 and not for chitosan, this treatment allows to remove PA6 from the surface of the films. Indeed, a pure PA6 film dissolves rapidly and completely when immersed in *m*-cresol;
2. a second set of samples was immersed in a buffer solution (pH = 6) of chitinases for 2 h at room temperature;
3. after steps (1) or (2), films were then washed several times in *m*-cresol and water or only water, respectively;
4. irrespective of the previous steps, films were finally freeze-dried.

2.4. Dynamic mechanical analysis

Dynamic mechanical tests were carried out in the glass–rubber transition temperature range of PA6 with a spectrometer RSA2 from Rheometrics working in the tensile mode. Testing conditions were chosen in such a way that the observed behaviour strictly obeys the laws of linear viscoelasticity (the maximum strain ε was around 10^{-4}). The specimen was a thin rectangular strip with dimensions 30 × 3 × 0.1–0.5 mm^3, depending on the film thickness. The set-up measures the complex tensile modulus E^*, i.e. the storage component E', the loss component E'' and the ratio of these two components, i.e. $\tan\phi$ ($= E''/E'$). In the present work, results are displayed as E' and E''. Measurements were performed under isochronal conditions at 1 Hz, and the temperature was varied between 300 K and 400 K in steps of 3 K. In order to remove most of the moisture, all materials were dried at 127°C (400 K) for 15 min under vacuum, immediately before experiments. It has been checked that under these conditions, the behaviour is not modified by further heat-treatment.

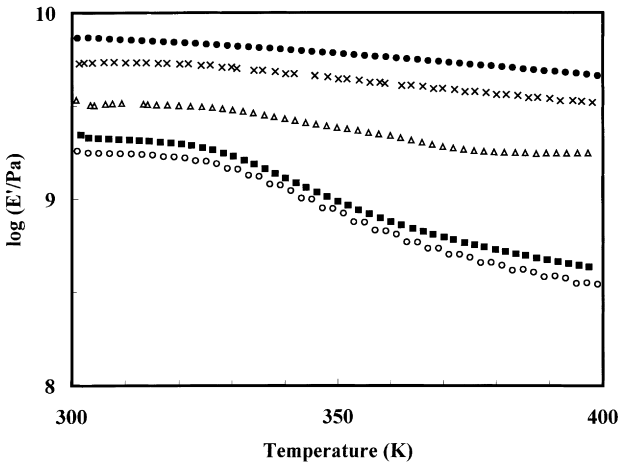

Fig. 1. The storage tensile modulus versus temperature at 1 Hz for (◦) 100/0 (pure PA6), (■) 85/15, (Δ) 50/50, (×) 30/70 and (•) 0/100 (pure chitosan).

3. Results and discussion

Dynamic mechanical measurements were performed on all the samples (100/0, i.e. pure PA6 to 0/100, i.e. pure chitosan). The curves of log(E'/Pa) and log(E''/Pa) versus temperature in the range 300–400 K corresponding to 1 Hz are shown in Figs 1 and 2, respectively. Pure PA6 exhibits a relaxation process where E'' at 1 Hz passes through a maximum around 67°C (340 K) (see empty circles in Fig. 2). It is labelled α and corresponds to the main relaxation which is attributed to the inelastic manifestation of the glass–rubber transition. It leads to the storage modulus drop of about one decade in the temperature range 320–380 K (Fig. 1). The mechanism of the α relaxation involves cooperative motions of long-chain sequences. However, these motions are constricted by the crystalline domains.

In contrast, chitosan does not exhibit any relaxation process in the same temperature range (see filled circles in Fig. 2). As in many polysaccharides, the glass–rubber transition cannot be reached without degrading chitosan. This is due to the high density of hydrogen bonds in most of the natural macromolecules. The modulus remains practically constant around 7 GPa, with a weak negative slope over the whole temperature range studied (Fig. 1).

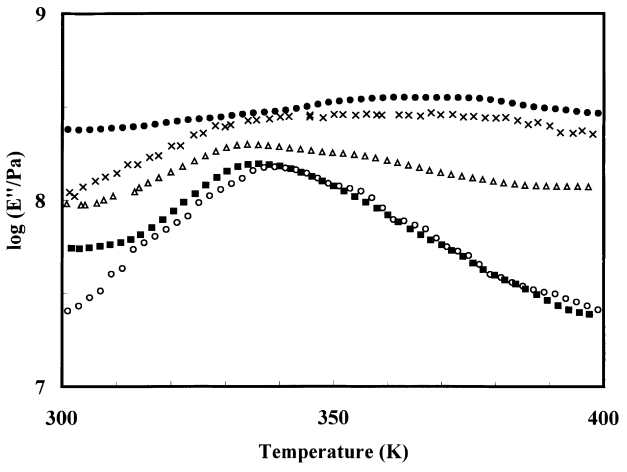

Fig. 2. The loss modulus versus temperature at 1 Hz for (◦) 100/0 (pure PA6), (■) 85/15, (Δ) 50/50, (×) 30/70 and (•) 0/100 (pure chitosan).

For the various blend compositions, E'' passes through a maximum in the same temperature range as pure PA6, but the magnitude of the α relaxation process decreases as the chitosan content increases. Two types of mechanical behaviour are displayed for these films from Fig. 1. First, those of the PA6-rich samples (100/0 and 85/15), which are characterized by a modulus drop of about one decade in the α relaxation zone. On the other hand, those of the remaining blends, for which the PA6 content is lower and the modulus drop practically does not exist. However, these results are insufficient to conclude on the blends morphology and additional information can be obtained from SEM observations.

The observations by SEM were made following the method described in Experimental (Section 2.3). Fig. 3 shows the surface of film 100/0 (pure PA6). The upper face (Fig. 3a) appears as an undulating surface notably

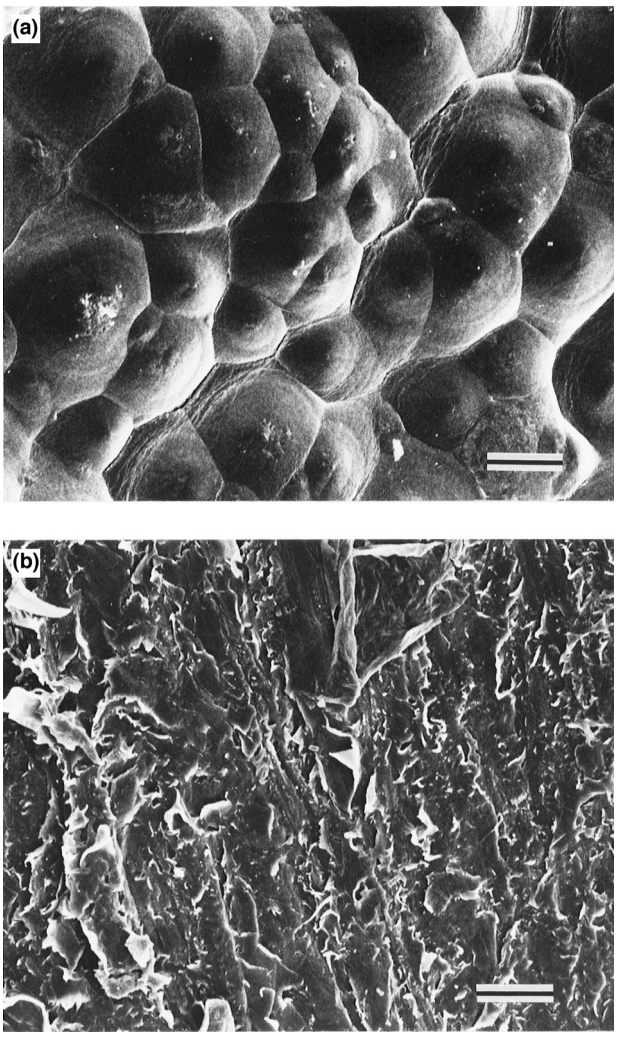

Fig. 3. Scanning electron micrographs showing (a) the upper and (b) the lower face of film 100/0 (pure PA6). Scale bar: 10 μm.

because of the evaporation step. In contrast, the lower face (Fig. 3b) is scored, probably because of the surface aspect of the boxes in which the blend solutions were cast. Polyamide film is not modified when it is immersed in a buffer solution of chitinases, whereas it is completely dissolved in *m*-cresol. The surfaces of film 0/100 (pure chitosan) is shown in Fig. 4. The same observations than those made for 100/0 film are reported, except the upper face, which is smoother than the upper face of PA6 film. In contrast with 100/0 film, pure chitosan is not modified when immersed in *m*-cresol, but it is completely degraded in the solution of chitinases. This is an indication that *m*-cresol is a good solvent of PA6 and not at all of chitosan, and that chitinases etch only chitosan, but not PA6.

Fig. 5 shows the surface of film 85/15, i.e. in which the bulk of the material consists of PA6, after etching by chitinases. It is relevant to note that SEM micrographs of all as-received blends, whatever the composition, were similar to those of as-received film 100/0. In the micrographs shown in Fig. 5a, Fig. 5b, the presence of holes can be observed. They obviously correspond to the degradation of chitosan. It is noteworthy that these holes are regularly dispersed and that their size is greater for the lower face (Fig. 5b) than for the upper (Fig. 5a). This is an indication that blends of chitosan and PA6 form mainly a two-phase system. Moreover, for the 85/15 composition the continuous phase is formed by PA6 and the inclusions are chitosan domains, and the lower face of the film seems to present a higher chitosan content. This gradient of chitosan concentration is probably induced by the processing technique itself, and chitosan domains tend to sediment during the solvent evaporation step. This phenomenon is due to the difference between the density of chitosan ($\rho \approx 1.5$) and the one of PA6 ($\rho \approx 1.1$). A similar observation was reported for thermoplastic nanocomposites filled with wheat straw cellulose whiskers[14], and the behaviour of these materials was modelled by subdividing the sample into layers with different whiskers content, lying parallel to the film surface. This sedimentation phenomenon is of great importance to the mechanical behaviour of the blend.

It was not possible to observe the surface of film 85/15 after etching by *m*-cresol because after this treatment, the sample had lost its consistency and was completely dissolved.

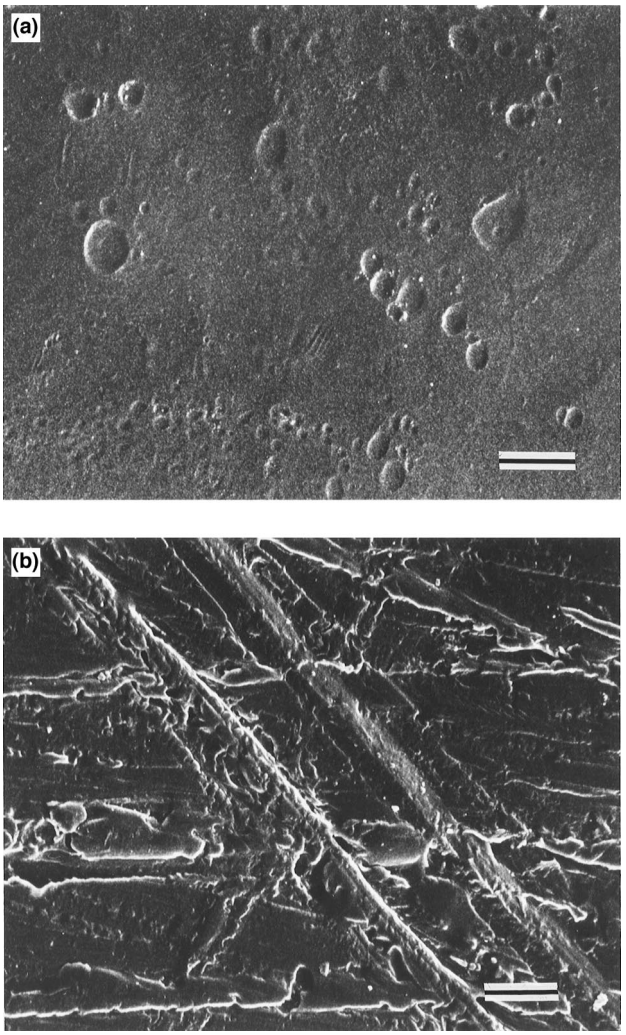

Fig. 4. Scanning electron micrographs showing (a) the upper and (b) the lower face of film 0/100 (pure chitosan). Scale bar: 10 μm.

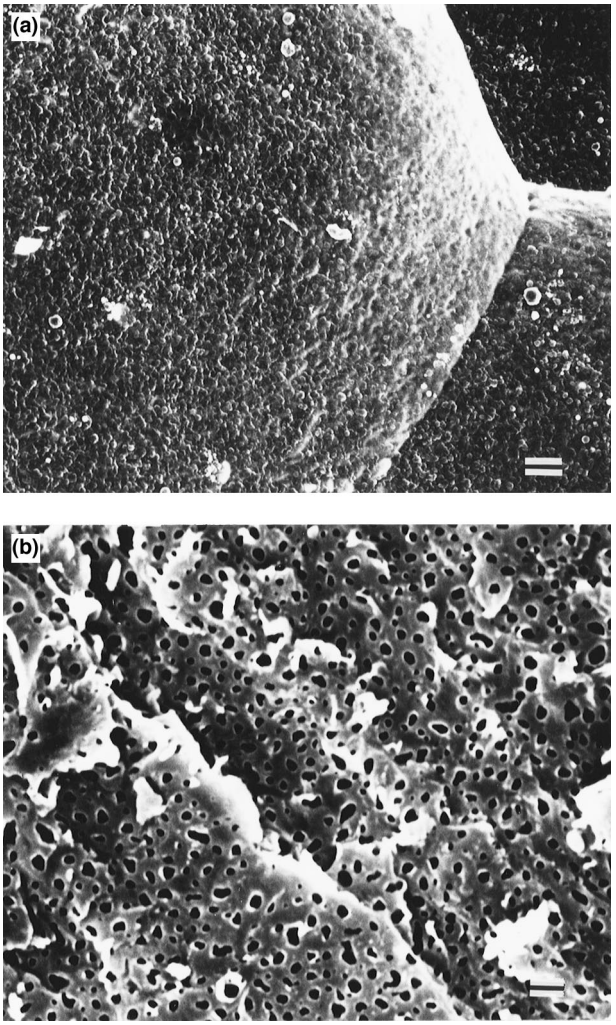

Fig. 5. Scanning electron micrographs showing (a) the upper and (b) the lower face of film 85/15 after etching by chitinases. Scale bar: 1 μm.

The surface of films 50/50 and 30/70 are shown in Figs 6 and 7, respectively. They were submitted to etching by chitinases (Fig. 6a, Fig. 6c, Fig. 7a, Fig. 7c), and by *m*-cresol (Fig. 6b, Fig. 6d, Fig. 7b, Fig. 7d). On the upper face of the films etched by chitinases (Fig. 6a, Fig. 7a), the presence of holes is attributed to the dissolution of chitosan. Their size is larger than it is for the 85/15 film (Fig. 5a), because of the greater chitosan content. They seem to be well dispersed on the surface. The lower face etched by chitinases (Fig. 6c, Fig. 7c) displays more and larger holes, corresponding to a higher chitosan content of the lower face compared to the upper one. This observation is in agreement with those previously reported for the 85/15 film.

Fig. 6b, Fig. 7b show the upper face of the 50/50 and 30/70 films, respectively, when immersed in *m*-cresol. These micrographs display the chitosan domains free from PA6. The opposite faces etched by *m*-cresol are shown in Fig. 6d, Fig. 7d, respectively. Contrary to the observations performed on the same etched 85/15 blend, the samples exhibit all the more consistency than the chitosan content is higher. Moreover, it is clear from comparison of Fig. 7b, Fig. 7d that the PA6 content, displayed by the presence of holes, is more significant on the upper face than it is on the lower face.

All these observations prevail us to propose a PA6/chitosan phase separation section such as the one represented by the scheme displayed in Fig. 8. The chitosan phase tends to sediment and to form a continuous phase on the lower face of the film, if the chitosan content is high enough. This continuous phase is bristling with chitosan domain cones, which can emerge on the upper face of the film depending on the blend composition. The PA6 rich domains fill the upper face of the sample.

In order to confirm these observations and to validate the proposed blend morphology it is of interest to compare the experimental mechanical data to the predicted ones. In multiphase polymer systems, the relationship between the elastic moduli, the composition of the two components, and the morphologies (or geometrical arrangements of each phase) has been extensively studied. Several models have been

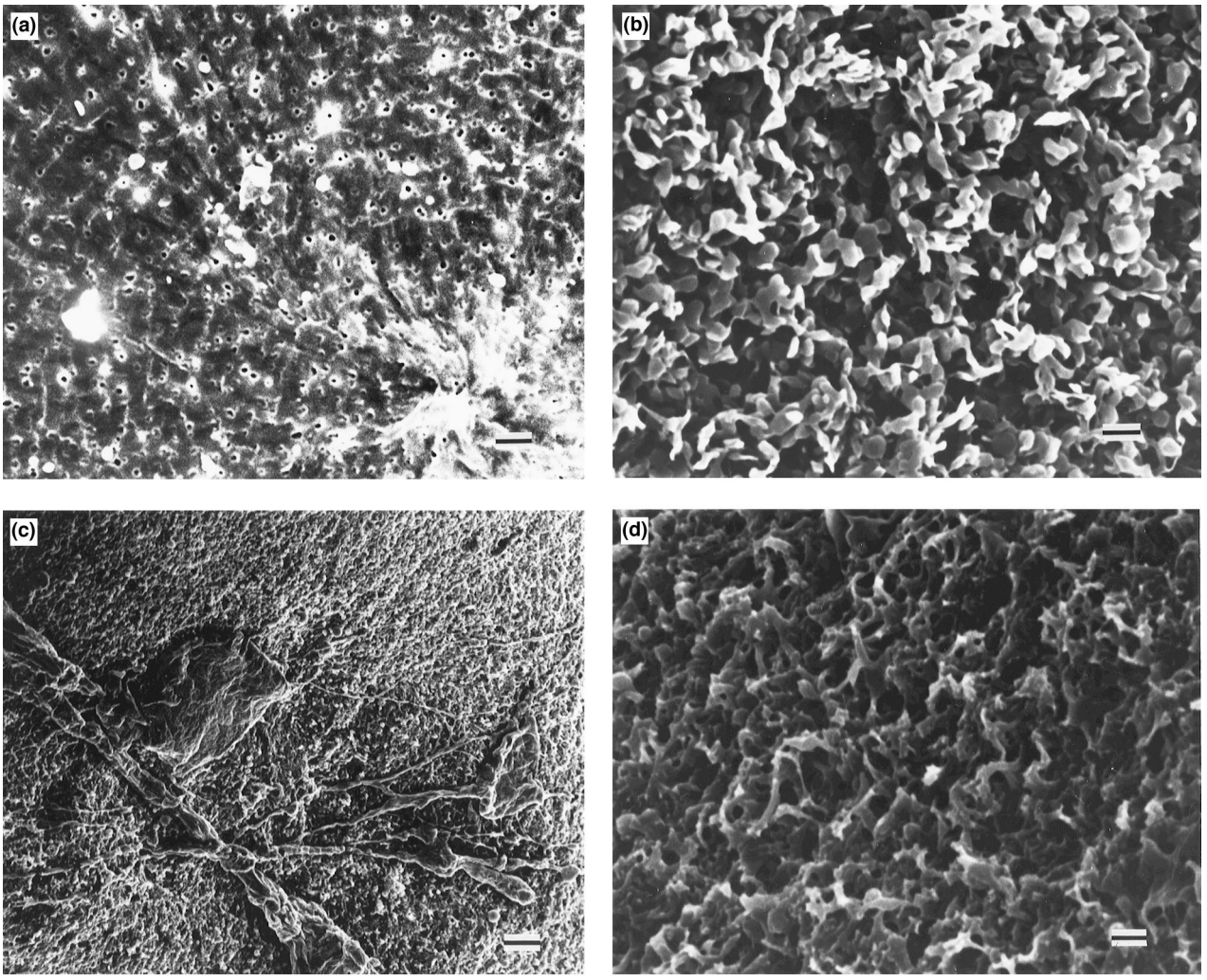

Fig. 6. Scanning electron micrographs showing the upper face of film 50/50 after (a) etching by chitinases and (b) etching by *m*-cresol, and the lower face of film 50/50 after (c) etching by chitinases and (d) etching by *m*-cresol. Scale bar: 1 μm.

developed to predict the mechanical behaviour of two phase systems such as blends of amorphous polymers[15–22] and to relate the modulus of these multiphase systems to their compositions and morphologies. Most theories assume perfect adhesion between the phases and the sample being macroscopically homogeneous and isotropic.

In previous works, a series–parallel model as proposed by Takayanagi[16] in which the concept of percolation is introduced[21] gave successful results when applied to cellulose/PA66[22] and to cellulose/PA6,69 blends[23]. It is a phenomenological model which consists of a mixing rule between the two simplest models involving connections in series (Reuss prediction) or in parallel (Voigt prediction) of the components. However, for blends of a rigid amorphous polymer (phase R with a glass rubber transition temperature $= T_{gR}$) and a soft semicrystalline polymer (phase S with a glass rubber transition temperature $= T_{gS}$) and for temperatures T in the range $T_{gS}-T_{gR}$, it is important to consider an approach in which the two parent polymers can percolate. Indeed, depending on the volume fraction of each constituent, both phases are able to shown a certain connectivity and the mechanical contribution of the soft semi-crystalline polymer (for temperatures higher than T_{gs}) to the blend behaviour is no more negligible. Therefore, a better prediction of the mechanical behaviour can be performed by using a 'three-branch' model rather than the classical 'two-branch' model[22].

A schematic diagram of the 'three branch' model is given in Fig. 9a where R and S refer to the rigid and soft phases, respectively, i.e. to chitosan and PA6 towards its glass–rubber transition. λ, ψ_R and ψ_S are the parameters of this mixing rule and $v_S = \psi_S + \lambda(1 - \psi_R - \psi_S)$ is the volume fraction of the soft phase. As developed elsewhere[22], ψ_R is the volume fraction of the rigid phase which has percolated, i.e. which really reinforces the material. Considering v_{Rc} and v_{Sc} as the critical volume fraction of phases R and S, respectively, at the percolation threshold, and b_R and b_S the corresponding critical exponents, ψ_R

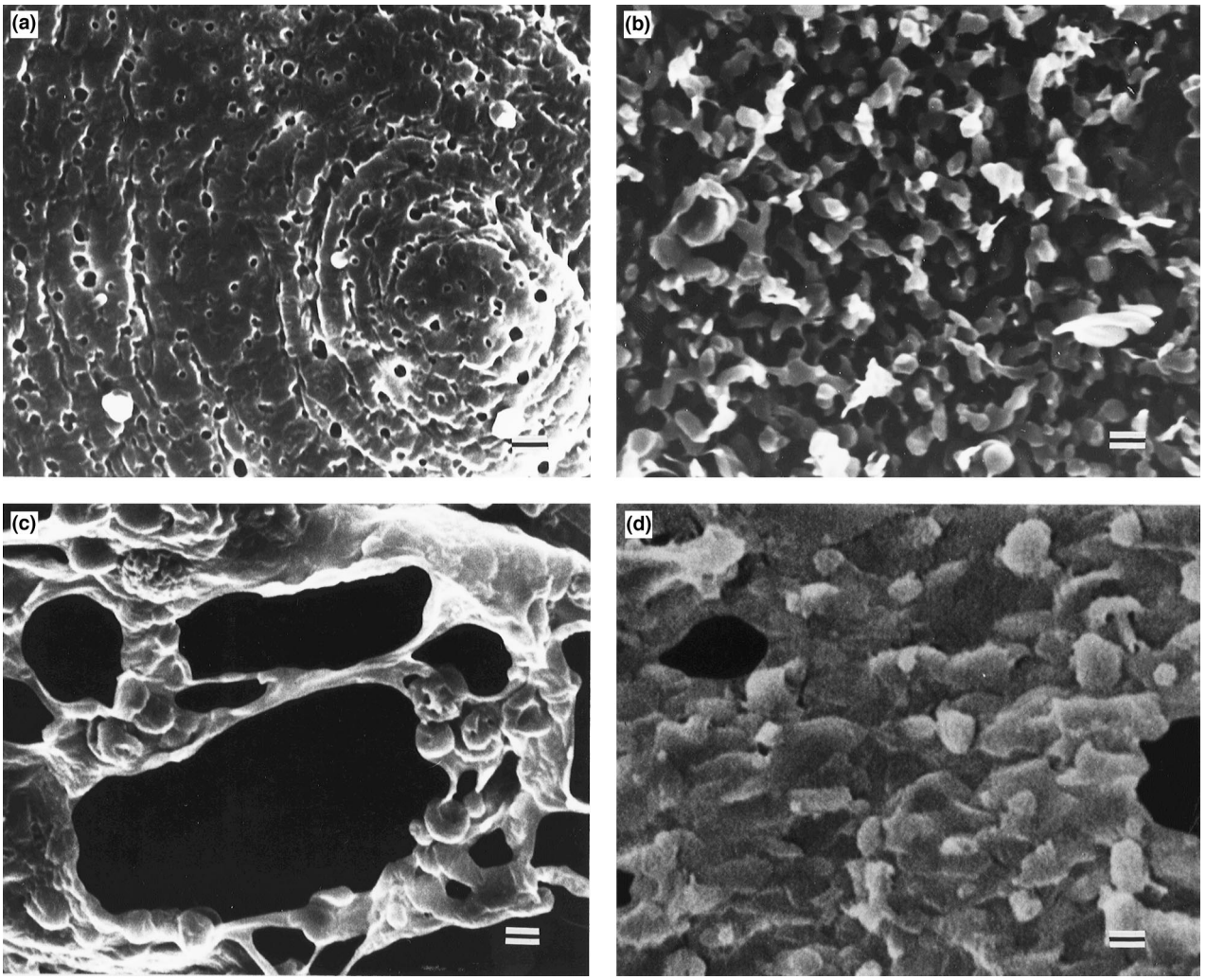

Fig. 7. Scanning electron micrographs showing the upper face of film 30/70 after (a) etching by chitinases and (b) etching by *m*-cresol, and the lower face of film 30/70 after (c) etching by chitinases and (d) etching by *m*-cresol; Scale bar: 1 μm.

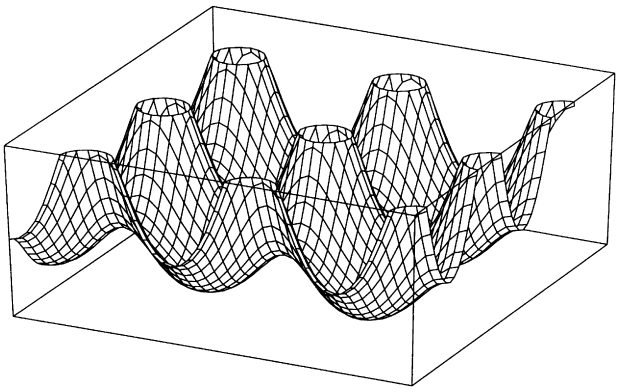

Fig. 8. Scheme of the morphology of the PA6/chitosan blends showing the phase separation.

and ψ_S can be written as:

$$\psi_R = v_R \left[\frac{v_R - v_{Rc}}{1 - v_{Rc}}\right]^{b_R} \quad \text{for } v_R > v_{Rc}$$
$$\psi_R = 0 \quad \text{for } v_R < v_{Rc} \tag{1}$$

and,

$$\psi_S = v_S \left[\frac{v_S - v_{Sc}}{1 - v_{Sc}}\right]^{b_S} \quad \text{for } v_S > v_{Sc}$$
$$\psi_S = 0 \quad \text{for } v_S < v_{Sc} \tag{2}$$

which are consistent with the fact that ψ_R and ψ_S should be equal to 1 when v_R and $v_S = 1$, respectively. Under a tensile situation the predicted modulus is given by (see ref. [22] for the full calculation):

$$E = \psi_S E_S + \frac{(1 - \psi_R - \psi_S)^2 E_R E_S}{(1 - \psi_R - v_S)E_S + (v_S - \psi_S)E_R} + \psi_R E_R \tag{3}$$

where E_R and E_S correspond to the tensile modulus of the rigid and soft phases, respectively. In fact, the behaviour of polymers is not purely elastic, but viscoelastic. For this reason, it is usual to modify the relationships for elasticity in introducing viscoelastic moduli (for each phase), i.e. under their complex form $E^*(i\omega,T)$[18,24]. The viscoelastic behaviour is obtained using the complex tensile modulus $E_S^* = E_S' + iE_S''$for the soft phase and $E_R^* = E_R' + iE_R''$ for the rigid phase as described elsewhere[22]:

$$E^* = \psi_S E_S^* + \frac{(1 - \psi_R - \psi_S)^2 E_R^* E_S^*}{(1 - \psi_R - v_S)E_S^* + (v_S - \psi_S)E_R^*} + \psi_R E_R^* \tag{4}$$

From Eq. (4) follows the expressions for E' and E'' given in Appendix A, corresponding to the complete three branch model, which will hereafter be denoted the 3B model. Though it is difficult to determine v_{Rc}, v_{Sc}, b_R and b_S [Eqs. (1) and (2)] as they depend on many parameters such as the geometry and the spatial distribution of each phase, we have considered that $v_{Rc} = v_{Sc} = 1 - v_{max}$, where v_{max} is the maximum volume fraction of rigid isoradius spheres, so that $v_{Rc} = v_{Sc} \approx 0.25$. The critical exponents b_R and b_S of the probability to obtain an infinite cluster are about 0.4 for the random sites percolation model[25,26]. The application of this model requires the knowledge of the experimental mechanical behaviour of the pure parent components: PA6 and chitosan.

Depending on the composition and then on the morphology of the blend, various arrangements of the three branches of the model schematized in Fig. 9a can be considered. One of the simplest models involves connections in series (Reuss prediction) or in parallel (Voigt prediction) of the components, and leads to the lowest lower bound or the highest upper bound for the moduli, respectively. The highest upper bound of the modulus is given by:

$$E^* = v_S E_S^* + (1 - v_S)E_R^* \tag{5}$$

This equation is applicable to a material in which two components are connected in parallel to the direction of the applied force. The lowest lower bound of the modulus is related to the model in which the two phases are connected in series, perpendicular to the applied force. The modulus prediction is then given by:

$$\frac{1}{E^*} = \frac{v_S}{E_S^*} + \frac{(1 - v_S)}{E_R^*} \tag{6}$$

Other possibilities consist in connecting in parallel the Reuss model and a volume fraction, ψ_R or ψ_S, of percolating rigid or soft phase, respectively. This leads to the predictions which will be labelled two branch R (2BR) model (see Fig. 9b) or two branch S (2BS) model (see Fig. 9c), respectively, in the present study. The corresponding storage and loss moduli, E' and E', are given in Appendix A

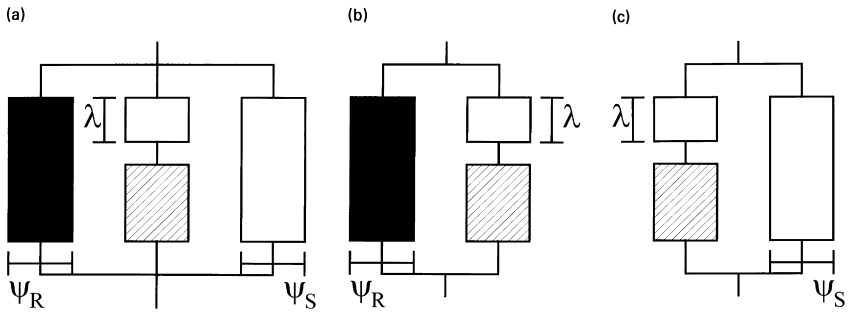

Fig. 9. Schematic diagram for the (a) 'three-branch' series–parallel model (3B), (b) two branch R (2BR) model, and (c) two branch S (2BS) model.

Calculated and experimental data are shown in Figs 10–12 for 85/15 to 30/70 blends. The calculated storage and loss moduli from the various predictions are shown in Fig. 10a, Fig. 10b, respectively, for the 85/15 blend, which also shows experimental results (filled circles). For this composition, the predictions of both Reuss and 2BR models are equivalent, owing to the fact that the volume fraction of rigid phase is lower than the percolation threshold v_{Rc}. The same observation can be reported for both 3B and 2BS predictions. It is clearly seen that fit is unsatisfactory in the case of Voigt model.This is an indication that no continuous chitosan phase is present in the blend. This phenomenon is in good agreement with the observations by SEM, because it was shown that 85/15 film had lost its consistency when etched in *m*-cresol.

In contrast, the storage modulus drop through the glass–rubber transition of PA6 and the associated maximum in the loss modulus are better described assuming either a Reuss (or 2BR) or a 3B (or 2BS) prediction. The difference between these two sets of models is the presence or the absence of the percolating PA6 phase, which plays a minor part on the mechanical behaviour of the blend, especially at high temperature. The vertical shift of the predicted moduli with respect to the experimental data is only due to the fact that the exact determination of the modulus depends on the precise knowledge of the sample dimensions. In fact, it was very difficult to obtain a constant and precise thickness along these samples besides the initial length between jaws was roughly measured. The uncertainty on the modulus value is also due to the small thickness of the films (10–50 μm).

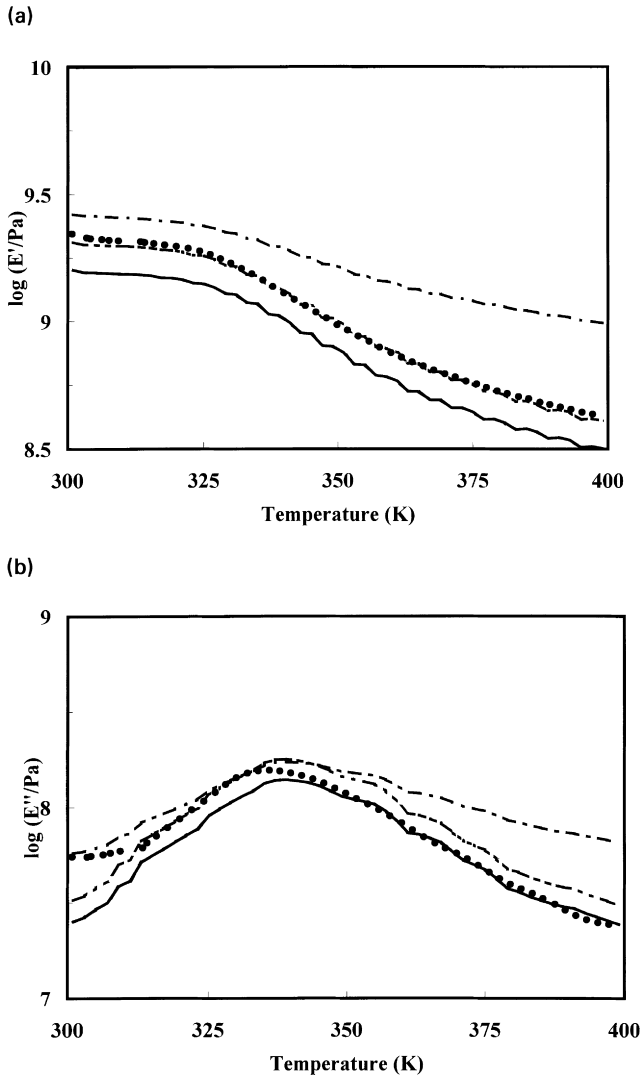

Fig. 10. Experimental (•) and predicted data from the Reuss model (- - -), the Voigt model (— – —), the 2BR model (— – – —), the 2BS model (— — —) and the 3B model (———), for (a) the storage tensile modulus and (b) the loss tensile modulus of the 85/15 blend. The same behaviour is predicted by the Reuss and 2BS models on the one hand, and by the 2BS and 3B models on the other hand.

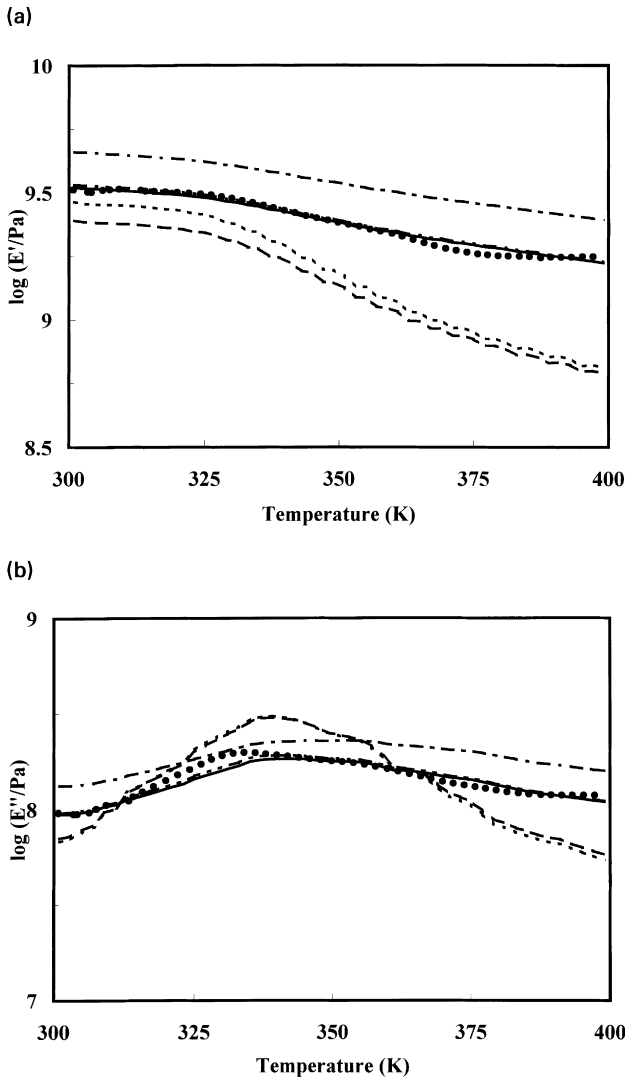

Fig. 11. Experimental (•) and predicted data from the Reuss model (- - -), the Voigt model (— – —), the 2BR model (— – – —), the 2BS model (— — —) and the 3B model (———), for (a) the storage tensile modulus and (b) the loss tensile modulus of the 50/50 blend.

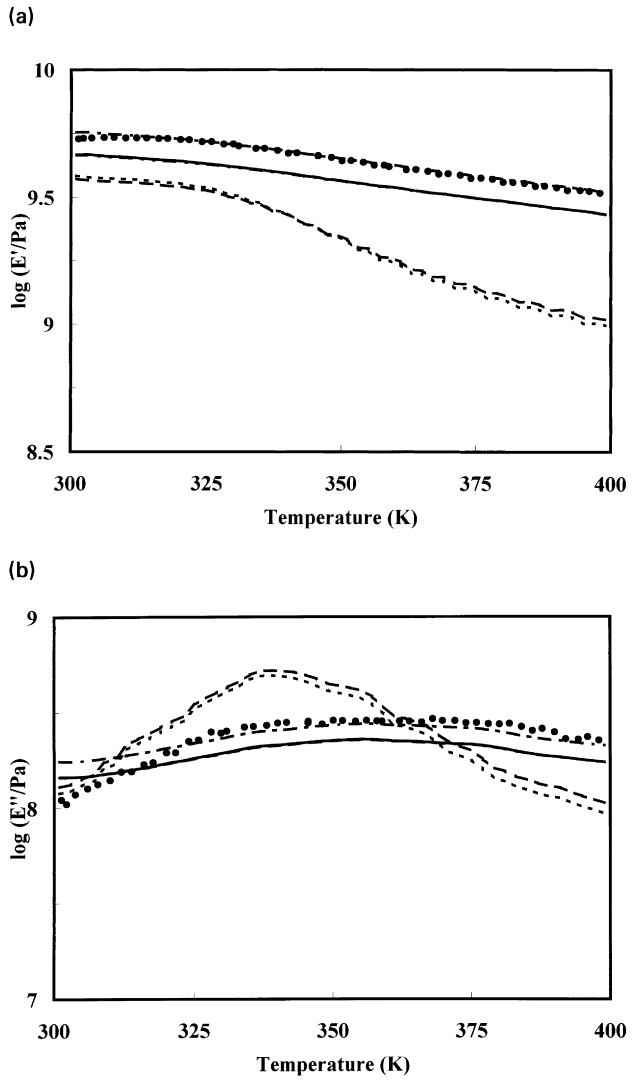

Fig. 12. Experimental (•) and predicted data from the Reuss model (- - -), the Voigt model (— – —), the 2BR model (— – – —), the 2BS model (— — —) and the 3B model (———), for (a) the storage tensile modulus and (b) the loss tensile modulus of the 30/70 blend.

The calculated and experimental data for the storage and loss components of the complex tensile modulus versus temperature are shown in Fig. 11a, Fig. 11b, respectively, for the 50/50 blend. The experimental behaviour is well predicted from the Voigt model, as well as from the 3B and 2BR models. As previously specified, the vertical shift of the prediction from the Voigt model with respect to the experimental data is only due to the uncertainty of the sample dimensions. On the contrary, the Reuss and 2BS predictions fail to fit the experimental data. This is a good indication that the chitosan domains percolate and form a continuous phase. According to the SEM observations, this continuous chitosan phase should be located on the lower face of the blend film. The same conclusions are reported for the 30/70 film (Fig. 12a, Fig. 12b), which mechanical behaviour is fairly well predicted from the Voigt model.

4. Conclusions

All the results obtained either by scanning electron microscopy (SEM) or dynamic mechanical analysis (DMA) lead to the conclusion that a phase separation occurs during the formation of films from the casting and evaporation of PA6/chitosan blend solutions.

Experimental data prevail us to propose a phase separation section, in which the chitosan phase tends to sediment and to form a continuous phase on the lower face of the film, depending on the blend composition. This continuous phase, if any, forms during the solvent evaporation step. The sedimentation phenomenon is clearly displayed by specific etching treatments before observation by SEM and it is of great importance to the mechanical behaviour of the blend. The continuous phase is bristling with chitosan domain cones, which can emerge on the upper face of the film if the chitosan content is high enough. The PA6 rich domains fill the upper face of the sample.

These observation are confirmed by DMA experimental data and from the modelling of the mechanical behaviour of the blends. It is clearly shown that no chitosan continuous phase exists when the chitosan content is 15 wt%, but it appears for richer chitosan compositions.

Appendix A

Calculation of the real and imaginary parts of the complex tensile modulus, according to the various models:

Voigt model:

$$E' = v_S E_S' + (1 - v_S) E_R'$$

$$E'' = v_S E_S'' + (1 - v_S) E_R''$$

Reuss model:

$$E' = \frac{v_S(E_R'^2 E_S' + E_S' E_R''^2 + E_R' E_R'' E_S'') + (1 - v_S)(E_R' E_S'^2 + E_R' E_R''^2 + E_S' E_R'' E_S'')}{[v_S E_R' + (1 - v_S) E_S']^2 + [v_S E_R'' + (1 - v_S) E_S'']^2}$$

$$E'' = \frac{v_S(E_R'^2 E_S'' + E_R''^2 E_S'' + E_R' E_S' E_R'' - E_R' E_S' E_R'') + (1 - v_S)(E_S'^2 E_R'' + E_R'' E_R''^2 + 2E_R' E_S' E_S'')}{[v_S E_R' + (1 - v_S) E_S']^2 + [v_S E_R'' + (1 - v_S) E_S'']^2}$$

Two branch R (2BR) model :

$$E' = \psi_R E'_R + (1-\psi_R)^2 \times \frac{v_S(E'^2_R E'_S + E'_S E''^2_R + E'_R E''_R E''_S) + (1-v_S-\psi_R)(E'_R E'^2_S + E'_R E''^2_S + E'_S E''_R E''_S)}{\left[v_S E'_R + (1-v_S-\psi_R)E'_S\right]^2 + \left[v_S E''_R + (1-v_S-\psi_R)E''_S\right]^2}$$

$$E'' = \psi_R E''_R + (1-\psi_R)^2 \times \frac{v_S(E'^2_R E''_S + E''^2_R E'_S + E'_R E'_S E''_R - E'_R E'_S E''_R) + (1-v_S-\psi_R)(E'^2_S E''_R + E''_R E''^2_S + 2E'_R E'_S E''_S)}{\left[v_S E'_R + (1-v_S-\psi_R)E'_S\right]^2 + \left[v_S E''_R + (1-v_S-\psi_R)E''_S\right]^2}$$

Two branch S (2BS) model :

$$E' = \psi_S E'_S + (1-\psi_S)^2 \times \frac{(v_S-\psi_S)(E'^2_R E'_S + E'_S E''^2_R + E'_R E''_R E''_S) + (1-v_S)(E'_R E'^2_S + E'_R E''^2_S + E'_S E''_R E''_S)}{\left[(v_S-\psi_S)E'_R + (1-v_S)E'_S\right]^2 + \left[(v_S-\psi_S)E''_R + (1-v_S)E''_S\right]^2}$$

$$E'' = \psi_S E''_S + (1-\psi_S)^2 \times \frac{(v_S-\psi_S)(E'^2_R E''_S + E''^2_R E'_S + E'_R E'_S E''_R - E'_R E'_S E''_R) + (1-v_S)(E'^2_S E''_R + E''_R E''^2_S + 2E'_R E'_S E''_S)}{\left[(v_S-\psi_S)E'_R + (1-v_S)E'_S\right]^2 + \left[(v_S-\psi_S)E''_R + (1-v_S)E''_S\right]}$$

Three branch (3B) model :

$$E' = \psi_S E'_S + (1-\psi_R-\psi_S)^2 \times \frac{(v_S-\psi_S)(E'^2_R E'_S + E'_S E''^2_R + E'_R E''_R E''_S) + (1-v_S-\psi_R)(E'_R E'^2_S + E'_R E''^2_S + E'_S E''_R E''_S)}{\left[(v_S-\psi_S)E'_R + (1-v_S-\psi_R)E'_S\right]^2 + \left[(v_S-\psi_S)E''_R + (1-v_S-\psi_R)E''_S\right]^2} + \psi_R E'_R$$

$$E'' = \psi_S E''_S + (1-\psi_R-\psi_S)^2 \times \frac{(v_S-\psi_S)(E'^2_R E''_S + E''^2_R E'_S + E'_R E'_S E''_R - E'_R E'_S E''_R) + (1-v_S-\psi_R)(E'^2_S E''_R + E''_R E''^2_S + 2E'_R E'_S E''_S)}{\left[(v_S-\psi_S)E'_R + (1-v_S-\psi_R)E'_S\right]^2 + \left[(v_S-\psi_S)E''_R + (1-v_S-\psi_R)E''_S\right]^2} + \psi_R E''_R$$

References

[1] Rathke TD, Hudson SM. J Macromol Sci Rev Macromol Chem Phys 1994;C34 (3):375.

[2] Muzzarelli RAA, Jeuniaux C, Gooday GW, editors. *Chitin in Nature and Technology*. New York: Plenum Press, 1986.

[3] Muzzarelli RAA. *Chitin*. In: *Naturally Chelating Polymers*. New York: Pergamon Press, 1973.

[4] Muzzarelli RAA. *Chitin*. New York: Pergamon Press, 1977.

[5] Zikakis JP, editor. *Chitin, Chitosan, and Related Enzymes*. Orlando, Florida: Academic Press, 1984.

[6] Blair HS, Guthrie J, Law T, Turkington P. J Appl Polym Sci 1987;33:641.

[7] Kim DY, Ratto JA, Blumstein RB. Polym Prepr 1991;31 (1):112.

[8] Zhao W, Yu L, Zhong X, Zhang Y, Sun J. J Macromol Sci Phys 1995;B34 (3):231.

[9] Ratto JA, Chen CC, Blumstein RB. J Appl Polym Sci 1996;59:1451.

[10] Paul D, Newman S. *Polymer Blends*, vol. 1. New York: Academic Press, 1978: 353.

[11] Olabisi O, Roberson L, Shaw MT. *Polymer—Polymer Miscibility*, New York: Academic Press, 1979.

[12] Cavaillé JY, Perez J. Makromol Chem Symp 1990;35/36:405.

[13] Gonzalez V, *PhD Thesis*, Universidad Autonoma de Nuevo Leon, Mexico, 1996.

[14] Dufresne A, Cavaillé JY, Helbert W. Polym Compos 1997;18 (2):198–210.

[15] Hashin Z. J Appl Mechan 1983;50:481.

[16] Takayanagi M, Uemura S, Minami S. J Polym Sci C 1964;5:113.

[17] Kerner EH. Proc Phys Soc 1956;B69:808.

[18] Dickie RA. J Appl Polym Sci 1973;17:45.

[19] Lewis TB, Nielsen LE. J Appl Polym Sci 1970;14:1449.

[20] Jourdan C, Cavaillé JY, Perez J. Polym Eng Sci 1988;28:1318.

[21] Ouali N, Cavaillé JY, Perez J. Plast Rub Compos Process Appl 1991;16:55.

[22] Garcia-Ramirez M, Cavaillé JY, Dufresne A, Tékély P. J Polym Sci Polym Phys 1995;33:2109.

[23] Garcia-Ramirez M, Cavaillé JY, Dufresne A, Dupeyre D. J Appl Polym Sci 1996;59:1995.

[24] Jourdan C, Cavaillé JY, Perez J. J Polym Sci Polym Phys 1989;27:2361.

[25] de Gennes PG. *Scaling Concepts in Polymer Physics*. Ithaca, NY: Cornell University Press, 1979.

[26] Stauffer D. *Introduction to Percolation Theory*, London, Philadelphia: Taylor and Francis, 1985.